Annals of Agrarian Science

Journal homepage: http://journals.org.ge/index.php

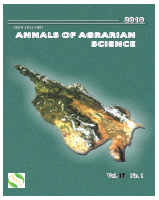

Forecasting Seasonal Rainfall Patterns for Crop Production in Juba County, South Sudan Using the Artificial Neural Networks

David Lomeling*, Salah Joseph Huria

Department of Agricultural Sciences, College of Natural Resources and Environmental Studies (CNRES), University of Juba, P.O. Box 82 Juba, South Sudan

Received: 5 June 2018; accepted: 12 September 2019

A B S T R A C T

A simple Multi-Layered Feed Forward (MLF) training process of the Artificial Neural Networks model with a learning back-propagation algorithm was applied to forecast rainfall data of Juba County, Central Equatoria State in South Sudan from 1997-2016. Annual rainfall data were aggregated into three seasons MAMJ, JAS and OND and later trained for best predictions for the period 2017-2034 using the Alyuda Forecaster XL software. Best training was attained once the *minimum error or cost function* of the weight $\Delta\omega$ was attained during gradient descent and expressed as Mean Square Error (MSE) and AE of the input variable. The results showed that for MAMJ and JAS months, the number good forecasts were over 97% whereas this was between 60-80% for OND months. The Seasonal Kendal (SK) test on future rainfall forecasts as well as the Theil-Sen slope showed a declining monotonic trend in the mean amounts in all three seasons with MAMJ, JAS at OND at 100, 150 and 80 mm respectively towards the end of 2034. Forecast of the Standardized Precipitation Index (SPI) showed that the MAMJ months for the years 2019 to 2027 will be moderately wet with near to normal drought except in April 2021 which will experience some severe wetness. Interdecadal severe drought is expected between 2028 to 2033 after almost two decades. The SPI of JAS and OND seasons will remain near normal to moderate drought during the same period. Declining onset of MAMJ rains is expected to significantly affect the timing for land preparation and crop planting. The forecast accuracy of the MLFFNN can be used as a vital tool for decision makers in projecting future rainfall and drought events.

Keywords: Artificial Neural Networks, Standardized Precipitation Index,Cumulative Distribution Function, Theil-Sen Slope Estimator Rainfall Forecasting, Precipitation Index, Drought Events.

*Corresponding author: David Lomelin; E-mail address: dr.david_lomeling@gmx.net

Introduction

Agriculture and more specifically crop production is the mainstay of much of the rural population of Juba County of Central Equatoria State (CES), South Sudan. It is predominantly rain-fed and therefore, sustainable crop production is not only contingent upon the frequency, intensity and magnitude of rainfall but also on the spatial-temporal variations. These factors all make rainfall predictions more challenging especially when coupled with the effects of climate change. Although no prior studies on the seasonality of rainfall distribution in CES have been conducted, experiential evidences from farming communities in the region over the last two decades report of clear deviations and decrease below average values and intensity especially during the onset of the rainy season (*Ja´be*). Generally, the annual onset of rain starts during the second to third dekad of April and continues till June punctuated with a dry spell around July. This then continues from August till October, significantly decreasing toward November and December dry season (*Méling*). The rainfall

pattern may be described as more or less bimodal in nature. Such belated occurrences of onset rains during this period over the last two decades could be attributed to the prolonged impacts of *El Niño*. The effects of such temporal shift from the traditional farming calendar caused by *El Niño* resulting to untimely availability of soil moisture [1] are often poor harvests or crop failure of crops like cowpea, maize or peanuts. Understanding such erratic rainfall events and assessing seasonal rainfall trends would require a better understanding of the effects of "*meteorological drought*" on the "*agricultural drought*". The former is expressed entirely based of the degree of dryness (usually related to rainfall anomaly from the long-term mean) whereas the latter is based on temporal soil moisture deficit during crop phenology coupled with intensive actual evapotranspiration.

Much of the rainfall predictions for South Sudan encompassing the study area of CES have in the last decade been issued by diverse regional and international institutions like the IGAD Climate Prediction and Applications Centre, (ICPAC); UN Food and Agriculture Organization (FAO); United Nations Office for the Coordination of Humanitarian Affairs (UNOCHA). These predictions are however, monthly with short decadal time-scales and often in the form of probabilities relative to monthly or seasonal rainfall averages. Spatial and temporal rainfall patterns do not often correlate with soil moisture contents and dynamics. [2] showed that surface soil moisture dynamics generally follow rainfall patterns at the two gravel plain sites, whereas this was not the case soil moisture dynamics in the sand dune site. Therefore, depending on intensity of rainfall, soil structure, surface sealing and infiltration, clear distinctions between meteorological and agricultural droughts should be made and how both are interlinked.

Developing drought risk insurance models for any country in sub-Sahara Africa where drought accounts for about 40% of the economic losses to smallholder farmers [3], would be of paramount significance especially, if the ANN training of historical data and subsequent prediction were based on shorter hourly or daily time scales. Other indices e.g. Soil Moisture Deficit Index (SMDI) [4] or the Normalized Soil Moisture Index (NSMI) [5] may be more appropriate indices than the SPI in developing drought risk insurance models as they directly capture the moisture status and available volumes of water in the soil. The Global Climate Observation System (GCOS) program has acknowledged soil moisture as one of the Essential Climate Variable (ESV SM) that will have to be routinely measured and monitored in space and time. In the last three decades, temporal and spatial in-situ soil moisture contents have continuously been measured through satellite-based soil moisture products obtained from active and passive microwave sensors like the Advanced Microwave Scanning Radiometer on Earth Observing System (AMSR-E) by [6] or the AQUA AMSR-E by [7]. Such geo-referenced soil moisture data would be used as input in ANN and in making spatial-temporal projections in drought risk insurance models.

In the last two decades, much research on rainfall prediction using the ANNs have been conducted in different parts of the world from monsoon summer rainfall using time series [8]; seasonal [9]; daily [10]; hourly [11]; dekadal [12]; monthly [13]. A comprehensive overview of ANNs use in temporal rainfall prediction has been reported by [14]. However, only a few similar studies have been conducted in Africa, in Ethiopia [15]; in Algeria [16] and in West Africa [17]. Other studies on predicting monthly tropical rainfall used hybrid linear stochastic with non-linear extreme machine learning method [18, 19]**.** Other researchers have applied linear stochastic methods e.g. autoregressive moving average ARMA for rainfall prediction [20]; Box-Jenkins SARIMA model [21] or predicting solid weekly waste generation using ANN and ARMA [22]; monthly river inflow using the seasonal autoregressive integrated moving average-adaptive neuro fuzzy inference systems (SARIMA-ANFIS) [23]; oil-gas production engineering [24,25]; in healthcare engineering [26]; image-based plant disease detection [27]; soil clay content mapping using hyperspectral image [28]; limited medical datasets [29]. Basically, the ANN is a type of Machine Learning (ML), whereby a computer-based model fed with historical data in a time series is trained to identify specific patterns and the derived "*intelligence*" later used to predict future events. Some major advantages of the ANN are its ability to: i) model nonlinear and complex relationships between input and output variables; ii) it can learn and make *generalization* from this input-output relationship. This learned processes can be used to

make inferences on previously unseen data, iii) it is not affected by *heteroscedasticity* and therefore does not impose any restrictions on the distribution of the input variable. This means, it can still model an input-output relationship irrespective of the non-constant nature of the variance in the time series.

to produce their respective outputs $f(\Sigma h_n)w_{hn}$. The total output ($\Sigma\Sigma\sigma_1$) is then the output of the entire ANN for that specific input (x_1) and is compared to the target value (σ_T). The difference is expressed as the measure of error (E) between the computed and expected values. The main

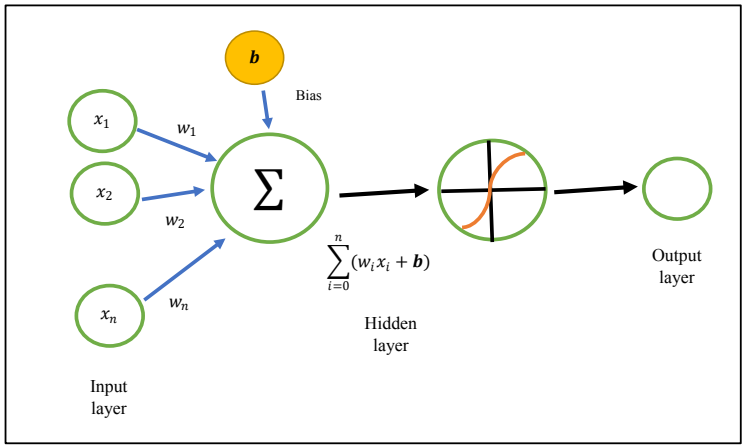

Fig. 1. *Simplified architecture of a feedforward two-layer ANN model with an input, hidden and output layer.*

However, one major drawback of the ANN is, its proneness to overfitting.

ANN Architecture

The neural network is based on a simplified and popularly used architecture called the Multi-Layer Feed Forward Neural Network (MLFFNN) as in Fig.1. Hereby, the product of the values of neurons or impulses $(x_1, x_2, x_3 \ldots . x_n)$ from the input layer and their respective weighted values $(wx_1, wx_2, w_{x3} \ldots . wx_n)$ are passed on to the middle neurons $(\Sigma h_1, \Sigma h_2, \Sigma h_3 \ldots . \Sigma h_n)$ in the hidden layer(s). Further, the products from the individual neurons in the hidden layer(s) $(\Sigma h_1, \Sigma h_2, \Sigma h_3 \ldots . \Sigma h_n)$ and the weighted sum of their respective inputs are passed on upon activation through a *transfer or logistic function* advantage of this MLFFNN model is that, the process of back propagation from the output to the hidden layer ensues and continues iteratively depending on margin of error till a minimum error value is attained.

Standard Precipitation Index, SPI

The Standardized Precipitation Index (SPI) is a popularly used index to characterize meteorological drought [30], on varying timescales. SPI is a probability index based entirely on precipitation as input variable. Formulated by [31] it can better represent rainfall anomalies in terms of wetness or drought than for example the Palmer Drought Severity Index (PSDI).

Table1. *Classification scale for the SPI*

Drought		**Wetness**	
Description	**SPI**	**Description**	**SPI**
Extreme drought	< -2.0	Extreme wetness	>2.0
Severe drought	-1.5 to-2.0	Severely wet	1.5 to 2.0
Moderate drought	-1.0 to -1.5	Moderately wet	1.0 to 1.5
Near normal	-1.0 to 0.0	Near normal	0.0 to 1.0

The first step in calculating the SPI is to determine a Cumulative Distribution Function (CDF) that describes the long-term time series of precipitation observations in either 1, 3, 6-month, etc. intervals. The CDF with mean zero (*corresponds to the median precipitation*), is then applied to the cumulative probability and the SPI estimated. For a given time-scale, SPI values are positive for greater than and negative for less than median precipitation. The magnitude of the SPI departure from zero is a probabilistic measure of the severity of a wet or dry event that can be used for risk assessment. The time series of the SPI can be used for drought monitoring by setting application-specific thresholds of the SPI for defining drought beginning and ending times

Basically, the SPI was envisaged to express the spatial-temporal drought events and variability as influenced by rainfall deficit. It is defined as the number of standard deviations from which normally distributed random variable deviates from its long-term mean. Generally, precipitation whether monthly, seasonally or otherwise are not normally distributed and therefore, an equiprobability transformation is performed such that the derived SPI values follow a normal distribution with mean = 0 and standard deviation = 1. This is obtained by fitting a gamma function $\Gamma(\alpha)$ of the cumulative distribution to precipitation values in the time series (*as in our study a 3-month period*). For most part, the SPI estimates were let to vary between -2.0 and +2.0 which contained approximately 95% of the SPIs values with close to 68% within the range -1 to +1.

In our study therefore, we attempted to use a simple Multi-Layer Perceptron model of the artificial neural network in predicting rainfall patterns for crop production for the period 2016-2033. We evaluate its relevance in forecasting "*lumped*" seasonal precipitation derived from historical data after training and testing.

Methodology

This study evaluated the significance of the ANNs in the forecasting of seasonal rainfall patterns in Juba County of Central Equatoria State (CES), South Sudan. In general, there are five basics steps: (1) collecting data, (2) preprocessing data, (3) building the network, (4) training and (5) test performance of model. The basic flow in designing ANNs model is given in Fig. 1. The daily rainfall data for Juba weather station as from the years 1983 to 2015 were downloaded from the US National Oceanic and Atmospheric Administration (NOAA). However, daily and consistent rainfall data were only recorded as from 1997 to 2016 and were used for this study. Data preprocessing involved aggregating the daily rainfall amounts to monthly means of March-April-May-June (MAMJ), July-August-September (JAS) and October-November-December (OND). Due to the unpredictable onset of rains especially between mid to end of March of each season, the MAMJ was "*lumped*" together. Rainfall around mid-March prior to the onset of the rainfall season in April was characterized by drizzles and light rainfall showers. With these monthly rainfall data sets, neural networks were then created and later proceeded by training and forecasting.

The chosen rainfall data for each season were divided into two random groups, the training and test sets corresponding to 82% and 18% respectively. Networks were trained for a fixed number of epochs or iterations till a minimum error function was reached. The optimal number of neurons in the hidden layer was obtained experimentally running the training process several times until a good performance was obtained or when no other changes were observed.

The Seasonal Kendall (SK) Test

The rank-based nonparametric Seasonal-Kendall method was applied to the long-term rainfall to detect any statistically significant trends. In this SK test and for the null hypothesis (H_0), assumed that there was no monotonic trend in precipitation amounts over time; and for the alternate hypothesis (H_1), it assumed that there was either an increasing or decreasing monotonic trend over time.

Once the seasonal rainfall data from 1997-2015 for MAMJ, JAS and OND months were trained and future forecasts made using neural network, test for the presence of any monotonic trend in the seasonal rainfall during the entire period between 1997 to 2034 was conducted using the Seasonal Kendall (SK) test [32,33,34]. The SK statistic for the *i-th* season S_i may be computed as:

$$\boldsymbol{S_i = \sum_{k=1}^{n-1} \sum_{j=k+1}^{n} sgn(x_{ij} - x_{ik}), \quad i = 1, 2, 3, \ldots n} \qquad (1)$$

$$sgn(x_{ij} - x_{ik}) \begin{cases} 1 \; if \; x > 0 \\ 0 \; if \; x = 0 \\ -1 \; if \; x < 0 \end{cases} \quad (2)$$

Where $sgn(x_{ij} - x_{ik})$ is the indicator function for the month (i) for the two respective years j and k. The SK statistic $\vec{S}$ for the entire series may be computed as:

$$\vec{S} = \sum_{i=1}^{n} S_i \quad (3)$$

A positive value of $\vec{S}$ would indicate that there is a positive monotonic trend and vice versa. This is the alternative hypothesis (H_α) whereas the null hypothesis (H_0) would suggest that there is no monotonic trend in the time series at $p < 0.05$. The value of $\vec{S}$ and Var ($\vec{S}$) may be used to compute the test statistic Z as:

$$Z = \begin{cases} \dfrac{\vec{S} - 1}{\sqrt{\text{Var}(\vec{S})}} & if \; \vec{S} > 0 \\ 0 & if \; \vec{S} = 0 \\ \dfrac{\vec{S} + 1}{\sqrt{\text{Var}(\vec{S})}} & if \; \vec{S} < 0 \end{cases} \quad (4)$$

The presence of a statistically significant trend is evaluated using the Z statistic. A positive value of Z indicates an upward trend and a negative value indicates a downward trend. Incorporating the Theil-Sen slope estimator to the SK test gives a better understanding of the magnitude (*change of unit per time*) of the slope. Generally, the slope Q between two successive values in a time series is expressed as:

$$Q = \frac{x_j - x_k}{j - k}, j \neq k \; and \; j > k \quad \text{for } i = 1,2 \ldots N \quad (5)$$

Where x is the value at the j and k-th interval for n observations and N = n(n-1)/2. The overall Theil-Sen estimator is the median of these N values of Q can then be expressed. Significant trends at either the 95% or 99% confidence intervals can then be computed with the confidence limits defined by M_1 and M_2. Derivation of these indices is referred to [35].

Cumulative Distribution Function (CDF) of gamma distribution

For some chosen rainfall season and time scale, the CDF $G(x)$ of a gamma distribution (Γ_α) is defined as:

$$G(x) = \frac{1}{\beta^\alpha \Gamma_\alpha} x^{\alpha - 1} e^{-\frac{x}{\beta}} \quad (6)$$

Where;

$$\Gamma_\alpha = \int_0^\infty e^{-t} t^{\alpha - 1} dt \quad (7)$$

Where $x > 0$ is the rainfall amount and the gamma distribution parameters $\alpha > 0$ as the shape and $\beta > 0$ the scale parameters and can be estimated through the Maximum Likelihood Estimation (MLE). First, a measure of the skewness (A) with median $m = 0.5$ of all (x_i) non-zero values in the rainfall time series and ($\overline{x_i}$) the arithmetic mean is estimated as:

$$\text{A} = \ln(\overline{x_i}) - \left(\sum_{i=1}^{n} \ln(x_i) \right) n \quad (8)$$

The values for the gamma distribution parameters can then be estimated as:

$$\tilde{\alpha} = \frac{1}{4A} \left(1 + \sqrt{1 + \frac{4A}{3}} \right) \quad (9)$$

$$\tilde{\beta} = \frac{\overline{x_i}}{\tilde{\alpha}} \quad (10)$$

Data pre-processing and training of the network

In order to enhance a faster convergence, the monthly input variables were normalized relative to the seasonal averages. The normalized values consistent with the sigmoid activation function were between 0 and 1. Since probability is between 0 and 1, the normalized values would give better predictions during training. The Alyuda ForecasterXL basically splits the data into two sets (1) training and validation sets (2) training set. During training, the weights of the neural network were adjusted whereas the validation increases the

accuracy by minimizing the error function (**E**) during iteration. The training stopped once the error function reached a global minimum. Finally, the performance of the network was evaluated on the test data set which had not been involved in the training process. In this study, the neural network was trained with 76, 56 and 55 datasets for the MAMJ, JAS and OND months respectively.

Model performance

The performance of the neural network was best done by using the linear regression coefficients (r^2) of the actual and forecasted data during training. Hereby, the regression coefficients for each season for the test period 1997-2015 were calculated for the entire dataset, as well as the best model predictive performance in terms of good and bad forecasts (*expressed relative to 100% highest accuracy*) for the training (P_{train}) and test (P_{test}) data respectively. As in our case, $r^2 \geq 0.9$, $P_{train} \geq 90\%$, $P_{test} \geq 70\%$ were considered as good model performance indicators within the error of tolerance as in (Table 2)

Similarly, prediction accuracy of the ANN was tested by using both the Mean Standard Error (MSE) and Absolute Error (AE) during training. AE is the absolute difference between the predicted and observed values.

Training using a single input variable (x_{ij} measured rainfall amount for the *i*-th training case at the *j*-th network output) for (n) observations in a time series was conducted and the best forecast or prediction ($\hat{x}_{ij}$) after each iteration was estimated by minimum *error function* denoted by the AE or MSE as:

$$\mathrm{AE} = x_{ij} - \hat{x}_{ij} \tag{11}$$

$$\mathrm{MSE} = \frac{1}{n}\sum_{i=1}^{n}\left(x_{ij} - \hat{x}_{ij}\right)^2 \tag{12}$$

In both cases, the error function (**E**) is directly dependent on the weight component (**W**) which in turn influences the learning rate (η). This is updated or changes iteratively during gradient descent as:

$$\Delta\mathbf{W} = \eta\frac{\partial\mathbf{E}(\mathbf{W})}{\partial\mathbf{W}} \tag{13}$$

The smaller the error function the better the prediction during the training process. A minimum of five training runs were done on the same data set to obtain the best MSE. Thereafter, the neural network was perceived to have learned and could then be used for making predictions for unknown data. Training parameters like number of hidden layers, stopping condition, iterations number, learning rate and generalization loss were estimated on trial-and-error basis for each dataset.

On a similar note, monthly SPI values were estimated from respective CDF curves of historical rainfall data from 1997-2015 These SPI were trained and predictions for the period from 2016 to 2034 subsequently made.

Results and discussion

Neural Network Performance

The trained JAS with smaller dataset (n=56) and single hidden layer appeared to outperform the MAMJ dataset with larger dataset (n=76) and two hidden layers demonstrating the difference in performance as influenced by data size. The variances for MAMJ (μ=0.252), JAS (μ=0.332) and OND (μ=0.345) were 0.01, 0.006 and 0.07 respectively. Comparing the variance effects on all datasets, there was a notable difference on learning especially of JAS and OND datasets with similar data size. The MAMJ and OND were characterized by high standard deviation (σ=0.266) and (σ=0.1) respectively, whereas for JAS, this was σ=0.076). However, all training sets achieved statistically significant performances ($r^2 \geq 0.99$) with number of good forecasts over 60%. Figure 2 shows a plot of MSE and AE vs iterations during training for the MAMJ, JAS and OND datasets for the years 1997-2015. The accuracy of both error function estimates showed steep gradients prior to 1000-th iteration till to convergence at global minima. During training of the MAMJ dataset for example, there was a sharp decrease of the MSE from about 0.016 to as low as 0.0007 while for the AE this was between 0.1 to 0.016. It is seen that both error functions were large at low iteration values decreasing till convergence and subsequently increasing with further iterations. The AE and MSE during training for OND was ten-fold larger that of either MAMJ and JAS. The learning rate (η) as measured by number of iterations to reach global minimum is fastest for OND at 1008 than for

JAS and MAMJ at 1625 and 1363 respectively. Low iteration number for OND would suggest, that the stochastic gradient descent algorithm effected larger step size parameter with large errors. This accounted for faster and poor learning rates and therefore, poor generalization. Conversely, smaller step sizes with smaller gradients resulted into larger number of iterations and comparatively lesser errors and better generalization. Better generalization was manifested by the comparatively higher percentage of good forecasts in the training sets of both MAMJ and JAS. Further, the rate of change of the error function ΔW as in Eq. (13) had a significant effect on the performance and accuracy of the ANN.

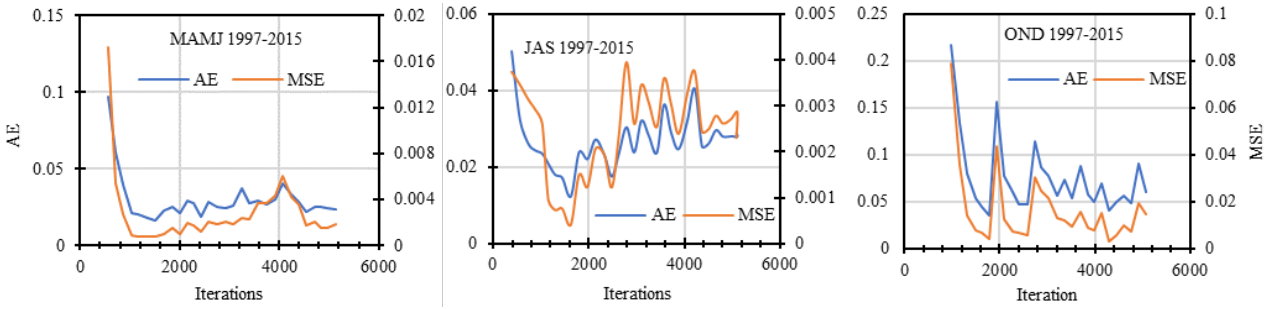

Fig. 2. *Error development and convergence to global minimum during training of MAMJ, JAS and OND of time series data between 1997 to 2015.*

Table 2 shows the training parameters and accuracy according to the r^2, number of good forecasts, hidden layer(s), MSE, and AE. The network demonstrated better performance rate for MAMJ and JAS when using two and one hidden layers respectively. The results here suggest, that model performance in terms of the number of good forecasts (98%) and approximation during validation for both seasons was independent of the number of hidden layers. In effect, one hidden layer performed just as good as two layers. Similar results on neural performance with a single hidden layer were reported by [36,37,38,39,40]. Although both JAS and OND trained datasets had each one hidden layer and almost equal data size, the latter gave a low number of good forecasts at 61% and high number of bad forecasts (39%).

Generally, better accuracy was shown by both MAMJ (2 hidden layers) and JAS (one hidden layer) trained data with a ten-fold less error than that of OND. However, training in terms of number of iterations needed for convergence, percentage of good and bad forecasts was observed in JAS dataset with one hidden layer, while the second best was MAMJ with two hidden layers. On the other hand, OND showed the highest inaccuracy with one hidden layer. This could be due to the inability to learn from a small dataset, although the learning logistic regression algorithm for JAS with similar data size seemed to work well. Similar observations were reported by [29,41]. Such conflicting generalizations in terms of the number of hidden layers for MAMJ-JAS as well as for JAS-OND on model performance and accuracy indicate striking instability especially for smaller datasets. For instance, using one hidden layer, the OND dataset had a learning rate of 0.0062 and reached the global minimum at lower iterations than JAS at 0.0021. After that, the error functions AE and MSE started to increase indicating that the model was getting over-fitted. Moreover, the MAMJ dataset with two hidden layers had a learning rate at 0.004 (Table 2) and was comparatively lower than that of OND but greater than that of JAS dataset with one hidden layer.

Conclusively, one can say, that the learning rate during gradient descent is inversely related to the number of iterations in reaching a global minimum. Judging by the rule-of-thumb in estimating the number of neurons in the hidden layer(s), our study showed that this was between 105 and 210 neurons for one and two hidden layers respectively for MAMJ dataset, whereas these were 99 and 100 neurons for OND and JAS datasets respectively. Despite such striking inconsistency between the JAS and OND datasets with the single hidden layer, the accuracy and generalization performance of the two-layer feedforward neural network model was satisfactory. With the error tolerance (%) as indicator for overall performance, the results demonstrate that, this model was able to achieve remarkable performances on predictive tasks with limited data size as in MAMJ and JAS datasets, but unable to perform well on smaller datasets as in OND.

Table 2. *Training parameters and network structures showing the goodness of error estimation between the training and test sets.*

	MAMJ		JAS		OND	
	Training set	**Test set**	**Training set**	**Test set**	**Training set**	**Test set**
Nr. of data set	63	13	47	9	46	9
AE	0.005	0.005	0.003	0.006	0.015	0.02
MSE	4.91E-05	2.35E-05	2.71E-05	7.42E-05	0.0003	0.0004
Error tolerance (%)	10	30	10	30	10	30
Nr. of good forecasts (%)	61(98%)	13(100%)	46(98%)	9(100%)	28(61%)	7(78%)
Nr. of bad forecasts (%)	2(3%)	0(0%)	1(2%)	0(0%)	18(39%)	2(22%)
r^2	0.994		0.996		0.997	
No. of hidden layer (s)	2		1		1	
No. of input layer (s)	1		1		1	
No. of output layer(s)	1		1		1	
Best at iteration number	1363		1625		1008	
Learning rate (η) till global minimum	0.0040		0.0021		0.0062	

Fig. 3 compares the performance of the linear-nonlinear method in predicting rainfall during training. The results show that both linear and nonlinear estimations had excellent abilities to forecast the seasonal rainfall amounts in the time series between 1997-2015. The average regression coefficient in the linear method was about (r^2=0.99). Although the actual and forecasted data during training seemed to give a high correlation and (r^2), it still showed some amount of error or noise as in (Fig. 2) for most part of the seasonal dataset trained. These errors were within the tolerance range put forth by the software. Hereby, the ANN model for rainfall forecasting may be assumed to be probabilistic and containing both deterministic as well as random error components. Therefore, both linear-nonlinear methods presented here during training of datasets can be regarded as good tools to be use for forecasting seasonal rainfall patterns

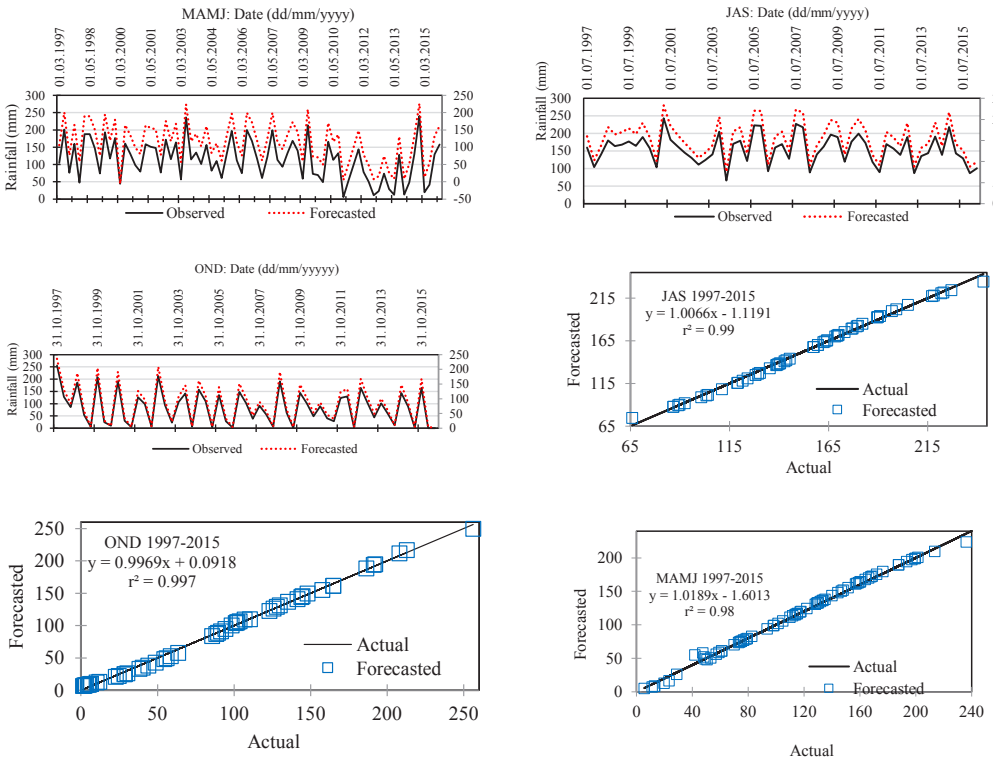

Fig. 3. *Scatter plots showing the correlation between the actual and forecasted data during training of neural network.*

Trends in mean seasonal rainfall and SK

Trained rainfall data for the MAMJ. JAS and OND months from 1997-2015 were used to forecast the mean rainfall over the period 2016-2034. Obtained results are shown in Fig. 4. The SK test *(S=-317; Z=0.774 and p=0.029*) showed a negative monotonic trend and statistically significant at 99% confidence level. The mean rainfall at the start of measurement for the MAMJ in 1997 was about 125 mm with about 5-10 mm reduction in 2015. This was a mean rainfall reduction of approximately 0.278 to 0.556 mm/year. Model projections from 2016-2034 forecasted a near 18% decrease in mean rainfall to about 100 mm. The total MAMJ rainfall reduction for Juba county between 1997 to 2034 is projected to be close to 32 mm. The JAS months also showed a decrease in the mean rainfall amount towards the end of 2034 forecasting period. The SK test (*S= -1171; Z= 1.901; p=0.234*) also showed a negative monotonic trend and statistically significant at the 95% confidence level. This was a slight 6-7% decrease from about 160 mm in 1997 to about 100 mm in 2034. The Theil-Sen slope Q* forecasted an annual drop of 0.2 mm/year which on average would be close to 7.64 mm as from 1997 to 2034. The OND also showed similar negative monotonic trend with SK test (*S= -317; Z=0.774; p=0.220*). There was a 21% decrease from about 95 mm in 1997 to about 75 mm forecast in 2034. The estimated Theil-Sen slope Q* value of 0.100 mm/year would be about 3.8 mm in 2034. Trend analysis in of all the seasons revealed a general decrease of rainfall in Juba County with highest decrease during the MAMJ and lowest in OND.

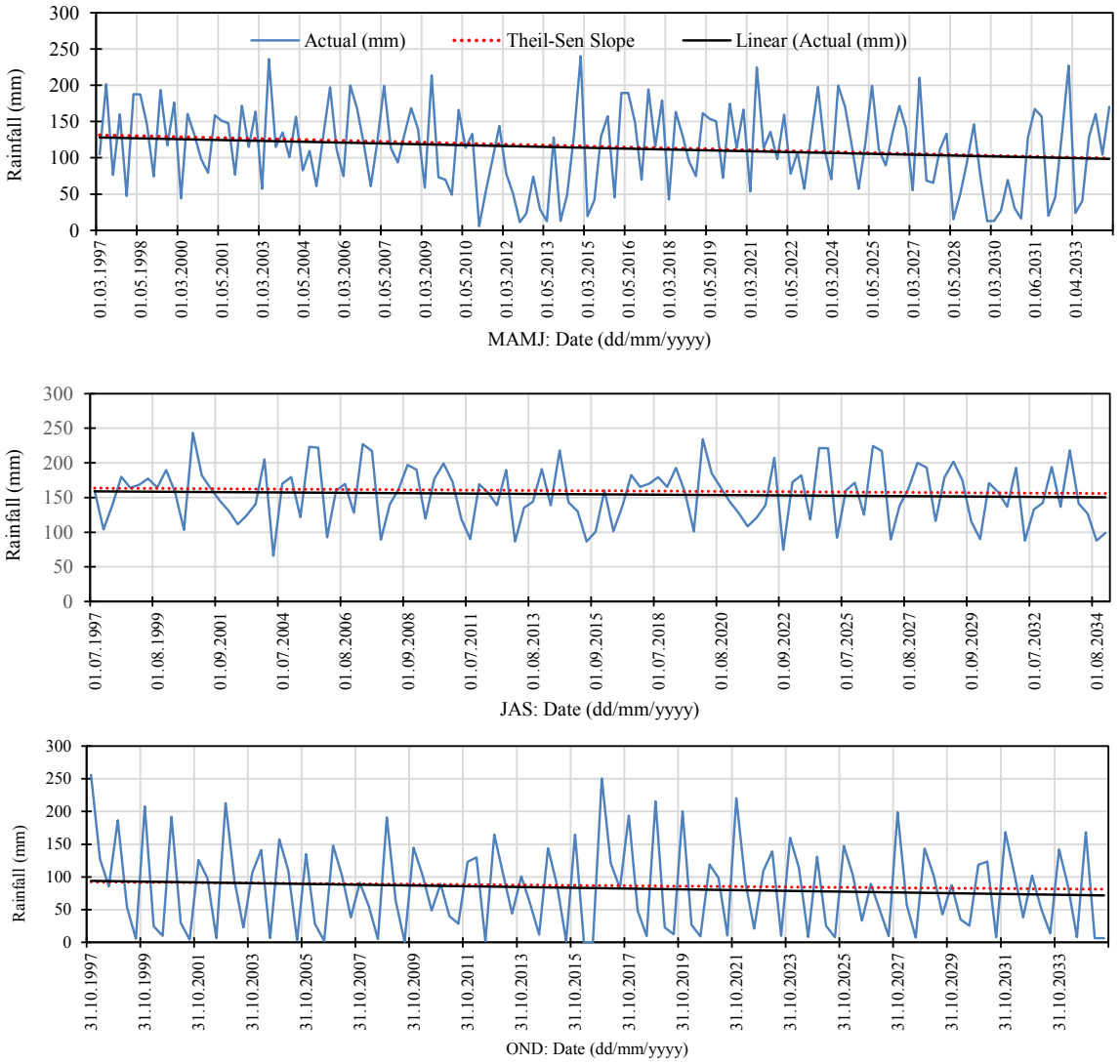

Fig. 4. *Ordinary Least Squares (OLS) Trendline (black line) of actual and the Theil-Sen slope (red-dotted line) between 1997-2034 for the MAMJ, JAS and OND months.*

Inter-seasonal SPI changes and drought

The histograms of the SPI during the MAMJ months is shown in Fig. 5. It was found that most of the MAMJ months of the preceding years from 1997 to 2016 showed near to normal to moderate wetness with similar drought SPI values. Recurrent severe drought for MAMJ months was witnessed during the years 2010-2013 with unusual extreme wetness in July 2014. However, the years 2015 till 2017 show normal to moderately wet MAMJ months. During 2018, the SPI for the AMJ months are expected to be near normal with moderate drought in March Table 3. It is forecasted, that the MAMJ months for the years 2019 to 2027 will be moderately wet with near to normal drought except in April 2021 which will experience some severe wetness (due to intensive rainfall). Interdecadal severe drought at SPI -1.5 to -2.0 with rainfall ranges less than 10th to 5th percentile is expected between 2028 to 2033 after almost two decades and is anticipated to have a long duration.

The SPI in July 2019 is expected to be about 0.6 with average rainfall of about 170 mm, while July 2019 with SPI 0.1 and about 150 mm. Occasional heavy rainfall downpour is expected between November/December 2019 despite the seasonal dryness during this period.

For the JAS months, 2018 is expected to be near normal Fig. 6. Sporadic and heavy rainfall is also expected during this period with 7-10 days of dry spells with absolutely no rainfall. In 2019, moderate drought in August with SPI -1.3 with rainfall range between 20th and 10th percentile is forecasted followed by severe wetness in September due to intensive rainfall that may cause serious flooding. However, inter-seasonal drought in September 2022 at SPI -1.9 is expected with rainfall range less than the 10th to 5th percentile. In our study, we found out that recurrent droughts in August followed by severe wetness in September is forecasted to continue till 2034. For the JAS months, no extreme drought is anticipated.

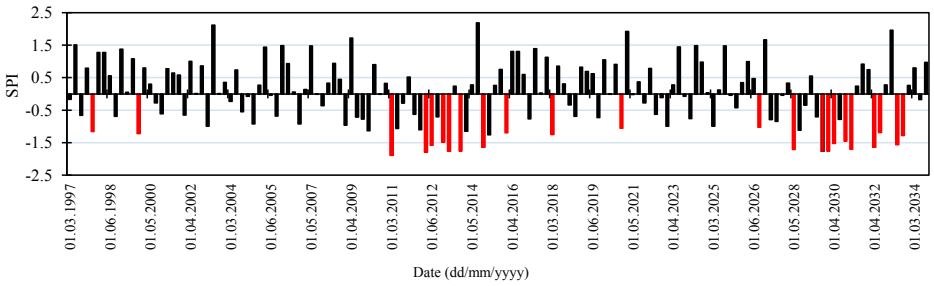

Fig. 5. *Calculated and projected SPI for the MAMJ months during the period 1997-2034*

Description	Month/Year
Moderate drought	03/2018, 03/2021, 03/2027, 04/2031, 05/2033
Severe drought	05/2028, 03/2030, 04/2030, 04/2032, 04/2033
Extreme drought	

Table 3. *Projected drought periods using SPI values from 2018 to 2034 for the MAMJ months*

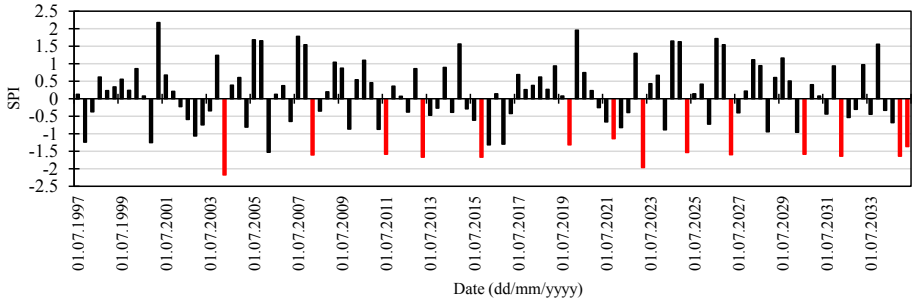

Fig. 6. *Calculated and projected SPI for the JAS months during the period 1997-2034*

Description	Month/Year
Moderate drought	08/2021
Severe drought	09/2022, 09/2024, 09/2026, 07/2030, 09/2031, 08/2034
Extreme drought	

Table 4. *Projected drought periods using the SPI values from 2018 to 2034 for the JAS months.*

For OND months, 2018 is expected to be remain near to normal with moderate drought at SPI -1.0 to -1.5 (rainfall range less than the 20th to 10th percentile) for much of the period except in October which is forecasted to be severely wet (Fig. 7). The cumulative effect of moderate drought especially during November and December months with SPI values between -0.93 to -1.1 respectively and rainfall probability between 10-20% or 20th to 10th percentile is expected to continue into the following new MAMJ season and significantly delay the onset of rainfall in March-April. This recurrent phenomenon will ostensibly interrupt the traditional farming-calendar especially during land preparation and sowing.

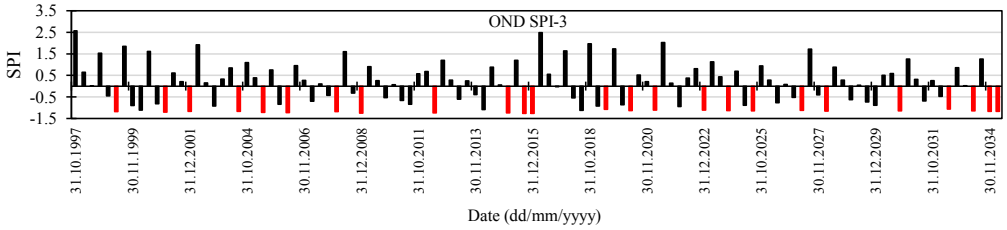

Fig. 7. *SPI histograms for the OND months in Juba County*

Changing rainfall patterns and impacts on crop production

Fig. 8 shows the anticipated decline in the amount of mean rainfall at the onset of rain during the MAMJ. The onset rains varied between the 4th dekad of February and 1st dekad of March with daily rainfall values generally below 4.0 mm level. The March rainfall amounts locally termed as *´doko kulunyit* (*that which carries away grass cinders after burning*) are barely enough for any effective land preparation and planting. Thus, most farmers tend to shift their land preparation and planting dates toward the 3rd and 4th dekad of April. Most farmers plant cowpeas (*ngete*), amaranth (*kwedekwede*), jute mallow (*mulukhiya/khudra*), okra (*bamia*) whose short growing and maturity periods (from 21 to70 days) often offers best food security options prior to the onset of the longer rainy JAS season. Increasing inter-seasonal rainfall variability with declining mean rainfall amounts during MAMJ is forecasted to continue, thus much crop production will have to be shifted toward the 4th dekad of April or 1st dekad of May while for maize, sorghum, sesame will have to be grown during the JAS to OND season. Mean onset rainfall amounts in 2018 is expected to be around 65 mm with a 25% probability. With declining amounts of the onset rains, there is need to intensify inter-cropping of fast and slow growing crops during the MAMJ-JAS seasons as much time, energy and water resources can effectively be utilized. These findings corroborate similar studies by [42] on declining rainfall trend in the March-May rains within the East African region.

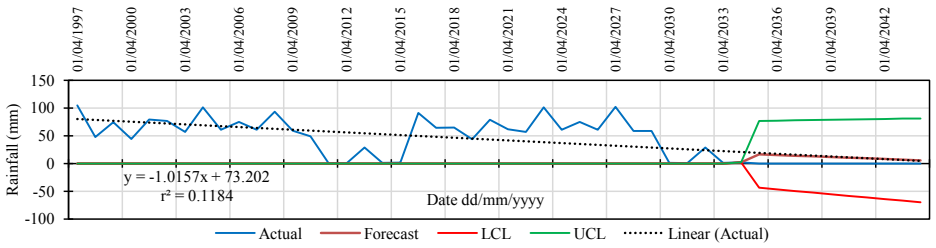

Fig. 8. *Observed and projected mean rainfall amounts during onset at first dekad of March (70 days from start of each new year where LCL=Lower Confidence Level and UCL= Upper Confidence Level).*

Interpretation of the gamma parameters (α) and (β)

Unlike the normal distribution curve that requires mean, median and mode to define the skewness, the gamma distribution requires that both the shape (α) and scale parameter (β) that are interlinked by Equation (10) be interpreted concurrently. For our study, we varied a *priori* the scale parameter (β) with different values around the mean values to observe the resultant effect on the shape parameter (α). The scale parameters for MAMJ, JAS and OND months with mean values of 113.32 mm, 154. 6 mm and 84.54 mm were 36.3, 30.6 and 77.3 respectively. We observed that a greater scale parameter *(with correspondingly low shape parameter*) had low ean and variance. Hereby, large scale parameter depicted large variability in rainfall patterns resulting in irregular rainfall typical for the comparatively drier OND months. Conversely, with increasing rainfall during the rainy season (Ja´be), the wetter JAS months with high mean and lowest scale parameter (*with correspondingly higher shape parameter*) showed low rainfall variability. The MAMJ months transitioning from the relatively drier OND months showed more, or less similar patterns to the JAS months with intermediate scale parameter and mean *(compared to JAS but higher than OND months*) that was often characterized by occasional rainfall showers in March prior to the onset of the rainy season in April. Hereby, the scale parameter was low with comparatively higher mean suggesting less rainfall variability and therefore wetness. With such interpretation of gamma parameters, it is likely to describe periods of relative wetness or dryness as well as drought-prone times.

For example, for the months JAS, the probability for normal wet conditions at SPI=0.5 increased with each scale parameter β as shown in Figs. 9 (a, c, e). The rainfall probability here at β=60.594 was about 0.56, at β=0.594 about 0.67 and at β=20.594 it was about 0.97. To illustrate the inter-linkage between scale parameter and rainfall amount at SPI=0.5 constant, a straight line was drawn from Fig. 9(a) that cut the cumulative rainfall in Fig. 9(b). The estimated rainfall amounts at β=60.594, β=30.594 and β=20.594 were about 140, 168 and 227 mm respectively and showed increasing rainfall amounts with decreasing scale parameter resulting into a more negatively skewed CDF. In general, this implies that wetter rainfall conditions have smaller β values than drier ones. This inverse relationship between scale parameter and rainfall amount may give insight into the rainfall patterns during anytime of the season as in the MAMJ and OND months

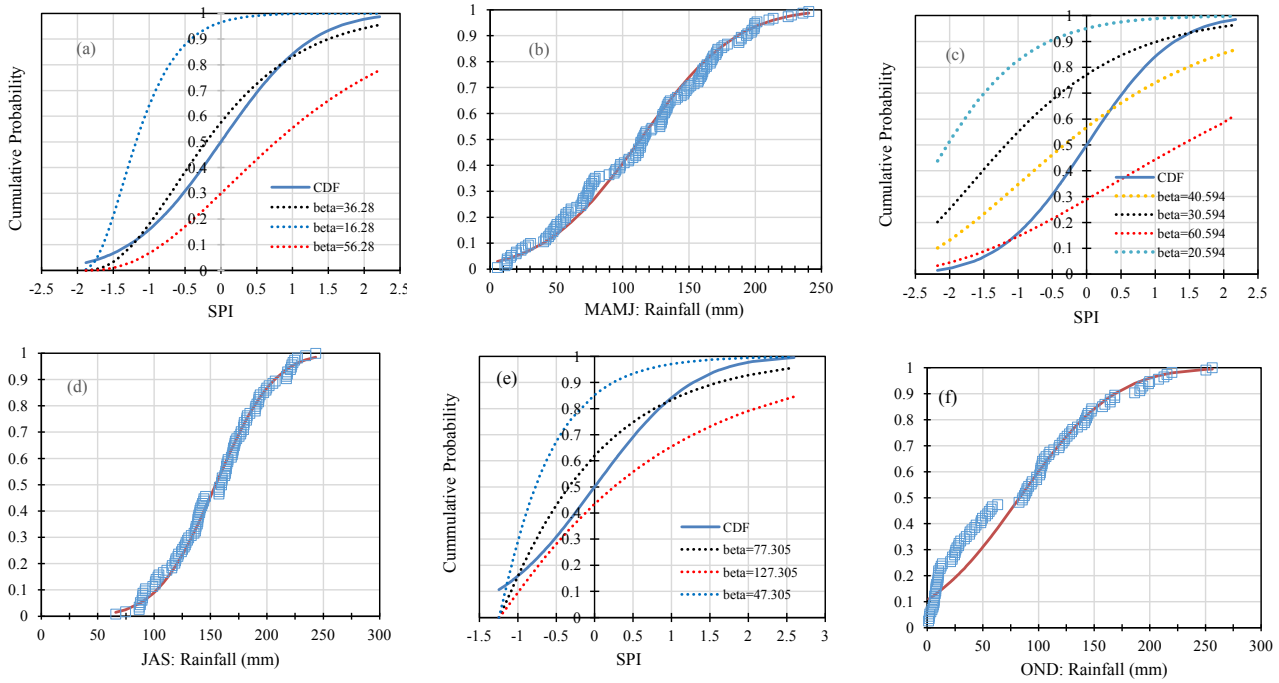

Fig. 9. *CDF plot of different shapes of the gamma distribution curves for the different seasons as influenced by different scale parameters β.*

SPI future projections

Fig. 10 shows the observed (1997-2016) and forecasted (2017-2034) SPI trends for the MMAJ, JAS and OND months. The results showed that the SPI decreasing trend of −0.15, -0.05 and -0.04 per decade for MAMJ, JAS and OND respectively was significant at p= 0.05. For JAS and OND this decrease in the next 100 years is forecasted to remain within the near to normal range while for MAMJ, this is forecasted to have moderate drought for the same period. In the short term, August 2019 is expected to be dry with SPI at about -1.3 (< 50 mm) and increase in September to about 2.0 (200 mm) and October at about 1.7 (<30 mm). November and December are expected to be dry with SPI at -0.8 (<30 mm) and -1.1 (< 25 mm) respectively. The reason is due to the low mean rainfall during OND coupled with high daily temperatures around this period that often continues into the MAMJ months prior to the onset of the first rainfall. Manufacturing industries and large-scale agricultural farming are practically non-existent in South Sudan and therefore, $C0_2$ or methane emissions due to "*anthropogenic compulsions*" are unlikely to be the causes for climate change and so changing rainfall patterns. However, the increased burning of fossil fuel, indiscriminate cutting down of forest trees as cheap energy source [1] over the last 50 years suggest a possible anthropogenic cause for the increase of dry events and thus reduced rainfall mean over Juba County. The results of our study on the negative trend of the SPI also suggest an overall shift of the SPI from near to normal towards more moderate drought events. This is coupled with occasional severe wetness characterized by flooding events especially during September-October months as anthropogenic compulsions continues to increase.

No conclusive reasons are accountable to the decreasing SPI trend with corresponding reduction in the mean rainfall amounts. However, the effects of global warming exacerbated by El Niño on rainfall patterns at the regional level may have occurred, but this could not be statistically identified and verified within the available historical rainfall data and time series.

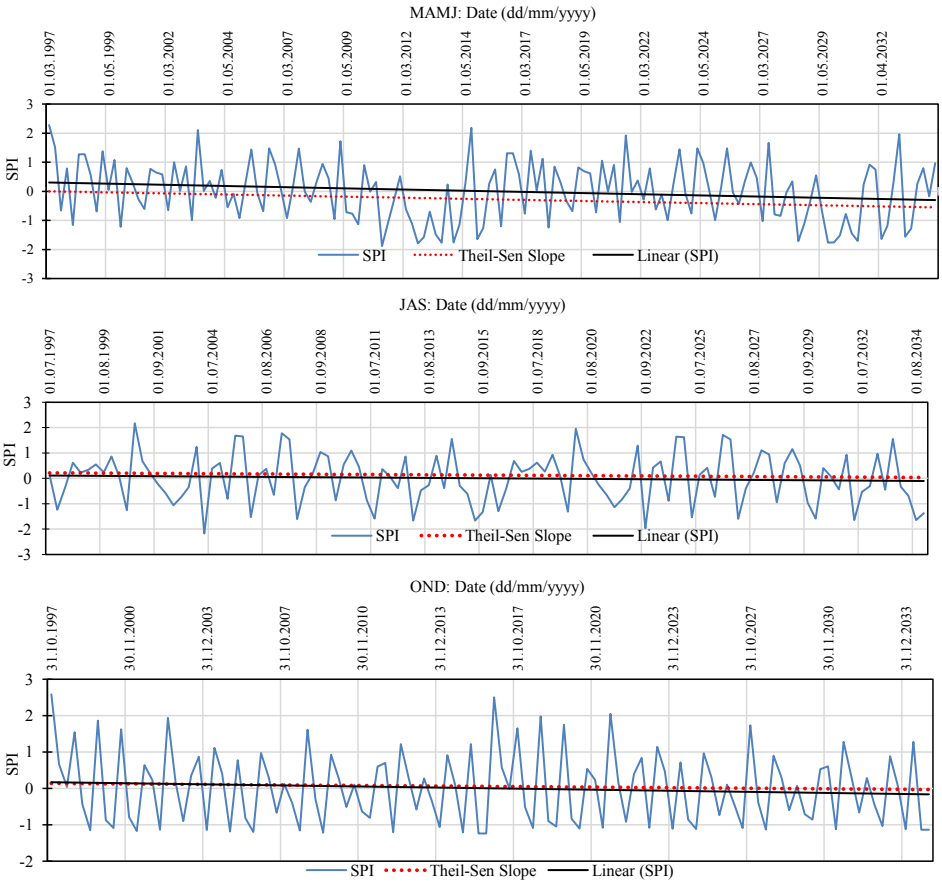

Fig. 10. *Measures SPI values (1997-2016) and projected SPI values (2017-2034) showing decreasing trend using the Theil-Sen Slope estimator.*

Conclusion

Time series rainfall data from 1997 to 2015 were trained, tested and used to make 3-months ahead forecast. Our study has shown, that the MLFFNN model with single input, hidden and output layers is a versatile tool in modelling and detecting complex nonlinear relationships and features between the input and output variables in a time series. After training of the respective datasets, the model was able to learn and generalize this relationship and thereby make predictions on future rainfall patterns for each season irrespective of the data size.

Rainfall and their subsequent projections to year 2034 using the ANNs showed that there was negative monotonic trend significant at the 99% confidence level for the MAMJ, JAS and OND months with rainfall amounts varying between 5-12% below seasonal averages. There was also decreasing trend in the average amounts during rainfall onset (*March-April*) with much rainfall events occurring towards the end 3rd and 4th dekad of April and in other instances in the 1st dekad of May of each year significantly affecting the timing for land preparation and subsequently planting.

Future SPI projections using the ANNs also showed that there was a decreasing trend in all the seasons or months with values forecasted to remain within the near normal range for JAS and OND months while for MAMJ forecasted to have moderate drought in the next 100 years. Rainfall amounts during these seasons are expected to be slightly below the seasonal averages with SPI values between 0 and -1.0. Hereby, national and state governments as well as development partners will be urged to prepare contingency and intervention plans that could quickly and timely be implemented to avert any disruptions to crop production.

However, challenges by the application of ANNs models in projecting spatial and temporal rainfall patterns especially on shorter hourly and daily time scales persist. Similarly, questions on the amount of historical data needed for training from which predictions can be made still pose huge challenges, especially in regions where such data are scanty. Understanding rainfall variability and intensity on hourly and daily basis within Juba County would increase the capacities and readiness of all stakeholders to timely and adequately respond to uncertainties arising from erratic rainfall patterns due to climate change. This paper recommends further studies to investigate whether such seasonal projections of rainfall can be corroborated with empirically measured rainfall amounts from several spatially placed stations within the county. However, one major disadvantage of this model is that in all datasets, the unusually high regression coefficients (r^2=0.99) between the observed and simulated was no panacea for model fitness alone, but simply highlighted the proneness to overfitting during training irrespective of error differences.

Conflicts of interest

None

Acknowledgment

The authors would like to thank the US National Oceanic and Atmospheric Administration (NOAAA) for availing valuable weather data for Juba, South Sudan. in their website, without which future rainfall predictions would be very difficult. We are also grateful to the USAID-funded project RHEA (Rebuilding Higher Education in Agriculture) hosted at the College of Natural Resources and Environmental Studies (CNRES) for providing us with a weather station. Hopefully, we shall will have it installed soon and start data logging.

References

[1] Lomeling D, Modi AL, Moti, SK, Kenyi MC, Silvestro GM, Yieb, JLL. Comparing the Macro-aggregate Stability of Two Tropical Soils: Clay Soil (Eutric Vertisol) and Sandy Loam Soil (Eutric Leptosol). International Journal of Agriculture and Forestry 2016; 6(4) :142-151.

[2] Li B, Wang L, Kaseke KF, Li L, Seely MK. The Impact of Rainfall on Soil Moisture Dynamics in a Foggy Desert. PLOS ONE 2016;11(10) e0164982. doi:10. 1371/journal.pone.0164982.

[3] Burke M, de Janvry A, Quintero J. Providing index-based Agricultural insurance to smallholders: Recent progress and future promise. Available at: http://siteresources.worldbank.org/EXTABCDE/Resources/7455676- 1292528456380/7626791-1303141641402/7878676-1306270833789/

Parallel-Session-5-Alain_de_Janvry.pdf. Accessed 18 Nov 2015.

[4] Narasimhan B, Srinivasan R. Development and evaluation of soil moisture deficit index (SMDI) and evapotranspiration deficit index (ETDI) for agricultural drought monitoring. Agric. For. Meteorol. 2005;133: 69–88.

[5] Dutra E, Viterbo P, Miranda PMA. Era-40 reanalysis hydrological applications in the characterization of regional drought. Geophys. Res. Lett. 2008;35, L19402.

[6] Njoku E, Jackson T, Lakshmi V, Chan T, Nghiem, S. Soil moisture retrieval from AMSR-E, IEEE Geosc. Remote Sens. Let., 2003;41(2):215–229, doi:10.1109/TGRS.2002.808243.

[7] Owe M, de Jeu R, Holmes T. Multisensor historical climatology of satellite-derived global land surface moisture, J. Geophys. Res.,2008; 113, F01002, doi:10.1029/2007JF000769.

[8] Singh P. Indian summer monsoon rainfall (ISMR) forecasting using time series data: A fuzzy-entropy-neuro based expert system. Geoscience Frontiers 2018;9: 1243-1257.

[9] Hartmann H, Snow JA, Su B. Seasonal predictions of precipitation in the Aksu-Tarim River basin for improved water resources management. Glob. Planet. Chang 2016;147:86–96.

[10] Devi SRP, Arulmozhiyarman C, Venktash C, Pramay A. Performance comparison of artificial neural network modelsfor daily rainfall prediction. International Journal of Automation and Computing 2016;13(5): 417-427.

[11] Hung, NQ, Babel MS, Weesakul S, Tripathi NK. An artificial neural network model for rainfall forecasting in Bangkok, Thailand, Hydrol. Earth Syst. Sci., 2009;13: 1413–1425.

[12] Warsito B, Gernowo R, Sugiharto A. Rainfall prediction by using wavelet general regression neural network. Int. J. Appl. Math. Stat. 2016;54(3): 32–41.

[13] Haviluddin M, Hardwinarto S, Sumaryono MA. Rainfall Monthly Prediction Based on Artificial Neural Network: A Case Study in Tenggarong Station, East Kalimantan – Indonesia. Procedia Computer Science 2015;59: 142 – 151.

[14] J. Abbot, J and J. Marohasy, J, Skilful rainfall forecasts from artificial neural networks with long duration series and single-month optimization. Atmospheric Research, 2017b;197: 289-299.

[15] Elsanabary MH, Gan TY. Wavelet analysis of seasonal rainfall variability of the Upper Blue Nile Basin, its teleconnection to global sea surface temperature, and its forecasting by an artificial neural network. Mon. Weather Rev. 2014;142(5): 1771–1791.

[16] Benmahdjoub K, Amour Z, Boulifa M. Forecasting of rainfall using time delay neural network in Tizi-Ouzou (Algeria). Terragreen 13 International Conference 2013-Advancements in Renewable Energy and Clean Environment. Energy Procedia 2013;36: 1138–1146.

[17] Badr HS, Zaitchik BF, Guikema SD. Application of statistical models to the prediction of seasonal rainfall anomalies over the Sahel. J. Appl. Meteorol. Climatol. 2014;3614–636.

[18] Zeynoddin M, Bonakdari H, Azari A, Ebtehaj I, Gharabaghi B, Madavar HR. Novel hybrid linear stochastic with non-Linear extreme machine learning method. J Environ. Manage.2018;15(222):190-206. doi: 10.1016/j.jenvman.2018.05.072.

[19] Ng JL, Aziz SA, Huang HF, Wayayok Y, Rowshon MK.Stochastic modelling of seasonal and yearly rainfalls with low-frequency variability. Stoch. Environ. Res. Risk A 2017;31: 2215–2233. https://doi.org/10.1007/s00477-016- 1373-9.

[20] Yaseen ZM, Ghareb MI, Ebtehaj I, Bonakdari J, Siddique R, Heddam S, Yusif AA, Deo R. Rainfall pattern forecasting using novel hybrid intelligent modelbased ANFIS-FFA. Water Resour. Manag. 2018;32(1): 105-122. https://doi.org/10.1007/s11269-017-1797-0.

[21] Osarumwense OI. Applicability of box Jenkins SARIMA model in rainfall forecasting: a case study of Port-Harcourt south Nigeria. Can. J. Comput. Math. Nat. Sci. Eng. Med. 2013;4: 1–4.

[22] Lomeling D, Kenyi SW. Forecasting solid waste generation in Juba Town, South Sudan using Artificial Neural Networks (ANNs) and Autoregressive Moving Averages (ARMA). Journal of Environment and Waste Management 2017;4(2): 211-223.

[23] Moeeni H, Hossein B, Ebtehaj I. Integrated SARIMA with Neuro-Fuzzy Systems and Neural Networks for Monthly Inflow Prediction. Water Resour Manage.doi 10.1007/s11269-017-1632-7.

[24]Khamis MA, Fattah KA. Estimating oil–gas ratio for volatile oil and gas condensate reservoirs: artificial neural network, support vector machines and functional network approach. Journal of Petroleum Exploration and Production Technology 2018; 1-10. doi. org/10.1007/s13202-018-0501-0.

[25] Mirzaie P, Salavati S. The Application of Artificial Neural Networks for the Prediction of Oil Production Flow Rate, Energy Sources, Part A: Recovery, Utilization, and Environmental Effects 2012;34(19): 1834-1843. dx.doi.org/2F 10.1080/2F15567036.2010.492386.

[26]Abiyev RH and Ma'aitah MKS. Deep Convolutional Neural Networks for Chest Diseases Detection. Journal of Healthcare Engineering Article ID 4168538 (2018) 11 https://doi.org/10.1155/2018/4168538

[27] Mohanty SP, Hughes D, Salathé M. Using Deep Learning for Image-Based Plant Disease Detection. Front. Plant Sci. 2016;7: 1419. doi: 10.3389/fpls.2016.01419.

[28] Liu L, Ji M., Buchroithner M. Transfer Learning for Soil Spectroscopy Based on Convolutional Neural Networks and Its Application in Soil Clay Content Mapping Using Hyperspectral Imagery. Sensors 2018; 18: 3169.doi:10.3390/ s18093169.

[29]Shaikhina T, Khovanova NA. Handling limited datasets with neural networks in medical applications: A small-data approach. Artificial Intelligence in Medicine 2017;75: 51-63). http:// dx.doi.org/10.1016/j.artmed.2016.12.003.

[30] Hayes M, Svoboda M, Wall N, Widhalm M. The Lincoln Declaration on Drought Indices: Universal Meteorological Drought Index Recommended. Bull. Amer. Meteor. Soc. 2011; 92: 485–488. doi: http://dx.doi. org/10.1175/2010BAMS3103.1.

[31]McKee TB, Doesken NJ, Kleist J. The Relationship of Drought Frequency and Duration to Time Scales. Eighth Conference on Applied Climatology, 17-22 January 1993, Anaheim, California.

[32] Hirsch RM, Slack JR, Smith RA. Techniques of Trend Analysis for Monthly Water Quality Data. Water Resources Research 1982;18(1): 107-121.

[33] Gilbert RO. Statistical Methods for Environmental Pollution Monitoring. Wiley, NY. 1987.

[34] Helsel DR, Hirsch RM. Statistical Methods in Water Resources Elsevier, NY. 1995.

[35] Salmi T, Maatta A, Anttila P, Ruoho-Airola T, Amnell T. Detecting Trends of Annual Values of Atmospheric Pollutants by the Mann-Kendall Test and Sen's Slope Estimates—The Excel Template Application MAKESENS; Finnish Meteorological Institute: Helsinki, Finland. 2002.

[36] Christiansen NH, Voie NH, Winther PET, Høgsberg OJ. Comparison of Neural Network Error Measures for Simulation of Slender Marine Structures Journal of Applied Mathematics Volume 2014, Article ID 759834, 11 pages. http://dx.doi.org/10.1155/2014/759834.

[37] Nakama T. Comparisons of Single- and Multiple-Hidden-Layer Neural Networks. In: Liu D, Zhang H, Polycarpou M, Alippi C, He H. (eds) Advances in Neural Networks – ISNN 2011. ISNN 2011. Lecture Notes in Computer Science, vol 6675. Springer, Berlin, Heidelberg.

[38] Sonntag ED. Feedback stabilization using two-hidden-layer nets. IEEE Transactions on Neural Networks 1992;3: 981–990.

[39] Lolli F, Gamberini R, Regattieri A, Balugani E, Gatos T, Gucc S. Single-hidden layer neural networksfor forecasting intermittent demands. International Journal of Production Economics 2016;183(A): (116-128). https:// doi.org/10.1016/j.ijpe.2016.10.021.

[40] Mahmoud O, Anwar O, Jimoh FESM. Learning Algorithm Effect on Multilayer Feed Forward Artificial Neural Network Performance in Image Coding. Journal of Engineering Science and Technology 2007;2(2): 188–199.

[41] Forman G, Cohen I. Learning from little: comparison of classifiers given little training. Proc. PKDD 2004;19: 161–72.

[42] Rowell DP, Booth BBB, Nicholson SE, Good P. Reconciling past and future rainfall trends over East Africa. J. Climate 2015;28: 9768–9788, https://doi.org/10.1175/JCLI-D-15-0140.1.